The incommensurate phases in the $Ta_{1-x}Nb_xTe_4$ charge-density wave system

1992 J. Phys.: Condens. Matter 4 2155

(http://iopscience.iop.org/0953-8984/4/9/010)

J. Phys.: Condens. Matter 4 (1992) 2155–2171. Printed in the UK

The incommensurate phases in the $Ta_{1-x}Nb_xTe_4$ charge-density wave system

J C Bennett†, S Ritchie†, A Prodan‡, F W Boswell† and J M Corbett†
† Guelph-Waterloo Program for Graduate Work in Physics, Waterloo Campus, University of Waterloo, Waterloo, Ontario, N2L 3G1, Canada
‡ J Stefan Institute, Jamova 39, 61000 Ljubljana, Slovenia, Yugoslavia

Received 28 October 1991

Abstract. A series of displacively modulated mixed crystals $Ta_{1-x}Nb_xTe_4$ ($0 \leq x \leq 1$) exist in which the modulation wavevector q varies as a function of composition. In this paper, the nature of the compositional dependence of q is studied in greater detail and evidence is presented for a stepwise variation of q with x. Electron diffraction experiments at room temperature reveal that the modulation periodicity remains commensurate until a threshold dopant concentration ($x = 0.3$) is exceeded and then jumps discontinuously to an incommensurate value. Further jumps in q are observed as the dopant concentration is increased. Models of the superstructures of the doped crystals corresponding to plateaux in the dependence of q on x are studied by comparison of the observed and calculated electron diffraction patterns. The results indicate that the mixed crystals may be described as a series of long-period commensurate superstructures. In addition, satellite dark-field microscopy has revealed the presence of defects in the modulation structures of the doped crystals, including antiphase boundaries and discommensuration arrays. The effects of substitutional doping on the phase transitions occurring on heating above room temperature in $TaTe_4$, and on cooling in $NbTe_4$, are also examined. The observations are interpreted in terms of the charge-density wave origin of the modulations.

1. Introduction

The transition metal tetrachalcogenides $TaTe_4$ and $NbTe_4$ possess a quasi-one-dimensional crystal structure in which chains of metal atoms are centred within extended cages of Te atoms in square antiprismatic coordination (figure 1). The presence of isolated one-dimensional chains of metal atoms renders these compounds susceptible to the onset of a charge-density wave (CDW) and the accompanying periodic lattice distortion. In $TaTe_4$, the lattice distortion results in a $(2a \times 2a \times 3c)$ commensurate superstructure [1, 2] at room temperature, while in $NbTe_4$ a $(\sqrt{2}a \times \sqrt{2}a \times \sim 16c)$ incommensurate modulation structure is observed [1, 3, 4], where a and c are the lattice constants of the tetragonal subcell. In addition to the room-temperature structures, several other modulated phases are stabilized upon heating or cooling. A transition to a $(\sqrt{2}a \times \sqrt{2} \times 3c)$ commensurate phase occurs in $TaTe_4$ on heating above 450 K [5] followed by a commensurate to incommensurate phase transition near 550 K [6]. In $NbTe_4$, a lock-in transition to a commensurate phase apparently isostructural with room-temperature

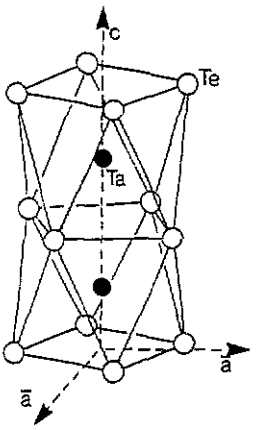

Figure 1. The tetragonal subcell of $TaTe_4$ and $NbTe_4$. The filled circles represent metal atoms while the open circles are Te atoms.

$TaTe_4$ occurs near 50 K [1, 7, 8]. Also, elongated streaks parallel to c^* in the electron diffraction patterns of $NbTe_4$ develop into sharp closely spaced spots on cooling below about 200 K and have been attributed to the presence of a new incommensurate phase or phases with basal dimensions ($2a \times 2a$) existing in the temperature range 50 to 200 K [9–11].

The wide variety of modulated structures and phase transitions occurring in the tetrachalcogenides, together with the relative simplicity of the subcell, has generated considerable interest in these compounds. Based on a Landau free-energy expansion of the form initially proposed by MacMillan [12], models of the room-temperature modulations in $NbTe_4$ and $TaTe_4$ have been developed by Walker and co-workers [13] 17]. One feature of the Landau approach is that, as a result of the competition between the elastic gradient terms in the free energy, which favour an incommensurate periodicity, and the anharmonic lock-in terms, which increase in relative importance at lower temperature, a discommensurate state is predicted prior to lock-in. The discommensurations are optimally phased in adjacent columns to minimize the overall free energy. Within this theoretical framework, the phase transitions, including the incommensurate to incommensurate transition occurring in $NbTe_4$ [15, 16] and the high-temperature commensurate to commensurate transition in $TaTe_4$ [17], are driven by temperature-dependent variations in the relative strengths of the interactions between CDW on first-, second- and third-neighbour columns.

Discommensuration arrays and their behaviour as a function of temperature have been observed in both $TaTe_4$ [6] and $NbTe_4$ [7–9] using satellite dark-field (SDF) microscopy. Although the details of the discommensuration process vary somewhat for the two compounds, the SDF images indicate that the discommensuration arrays evolve gradually from faults in the commensurate structures. Boswell *et al* [5] have shown that these faults arise from phasing errors of the CDW on adjacent columns associated with the structural transitions and may be considered as antiphase boundaries (APBS) in the commensurate modulation.

While the extensive number of theoretical and experimental studies of the tetrachalcogenides has resulted in a fairly detailed picture of the discommensurate state, the exact nature of the discommensurations occurring in the CDW modulations remains unclear. A high-resolution electron microscopy study of the room-temperature phase of $NbTe_4$ by Eaglesham *et al* [7] found little evidence of the phase slip expected for

discommensurations and concluded that the CDW modulation is very nearly purely incommensurate. The Landau theory approach suggests [18] that a very small energy contribution may be sufficient to pin the periodicity of an incommensurate CDW to a high-order commensurate value. Prodan *et al* [11], by comparison of the observed and computer-simulated electron diffraction patterns (EDP) have found that the structures of the two low-temperature $NbTe_4$ phases, denoted LT_1 and LT_2 (which become stable upon cooling $NbTe_4$ into the temperature range 200 to 50 K) as well as the room-temperature phase, are best described in terms of long-period commensurate superstructures.

The mixed crystal series $(Ta_{1-x}Nb_x)Te_4$ with $0 \leqslant x \leqslant 1$ provides an opportunity to investigate further the nature of the incommensurate phases. The initial study of this system revealed the existence of a complete range of solid solutions and a variation in the CDW modulation wavevector q as a function of composition [19]. A subsequent electron diffraction investigation found that the periodicity remains commensurate as x increases until a threshold concentration ($x \simeq 0.3$) is exceeded and then jumps discontinuously to an incommensurate value [20]. This was confirmed by the x-ray structural determination carried out by Kucharczyk *et al* [21] on the limiting commensurate composition $Ta_{0.72}Nb_{0.28}Te_4$. In this paper, the nature of the compositional dependence of the modulation periodicity is investigated in detail and evidence is presented from electron diffraction experiments for a stepwise variation with x. These observations provide the first indication of the occurrence of a 'Devil's staircase' [22] in a CDW modulated system. An extension of the analysis applied to model the LT_1 and LT_2 phases of $NbTe_4$ is used to investigate the structures of the mixed crystals corresponding to the apparent plateaux in the dependence of q upon x. The results of this analysis reveal that the mixed crystals, including the two end members $TaTe_4$ and $NbTe_4$, may be considered as a series of long-period commensurate superstructures.

As observed for $TaTe_4$ and $NbTe_4$, the mixed crystals undergo phase transitions upon heating and/or cooling with the nature of the transition being highly dependent on the stoichiometry. In addition, SDF images of the mixed crystals show the presence of numerous defects in the modulation superstructures, including discommensuration arrays and APBs. Thus, the study of the mixed crystals also provides further insight regarding the role of discommensurations in the commensurate to incommensurate transition process.

2. Experimental procedure

The crystals were grown by vapour transport in evacuated quartz tubes, using iodine as a transport agent, as described previously [1]. Following reaction at 900 °C for 24 h, the crystals were grown in a gradient of 700–500 °C for about 300 h. The tubes were then allowed to cool slowly in the furnace to room temperature. Specimens for electron microscopy were obtained by crushing the crystals between glass slides to produce a large number of crystallites with thin edges parallel to the chain axis. These crystallites were picked up on adhesive-coated copper grids. Examination was carried out on Philips CM20 and EM300 electron microscopes. *In situ* observations of the phase transitions were obtained using a single-tilt heating stage and a double-tilt liquid-helium cooling stage. The stoichiometry of the individual crystallites was determined by energy-dispersive x-ray microanalysis (EDX) using a probe diameter of 175 Å. The extrapolation

technique outlined by Van Cappellan [23] was used for the determination of the thin foil k-factors of Ta, Nb and Te.

3. Results

3.1. Observations at room temperature

3.1.1. Electron diffraction. In the EDPs, the presence of the CDW modulation is indicated by the presence of sharp satellite reflections located at $\pm mq$ (where m is an integer indicating the order) about the subcell reflections. For $NbTe_4$, all of these satellites may be indexed using a single incommensurate modulation wavevector $q = [\frac{1}{2}a^*, \frac{1}{2}b^*, 0.691c^*]$ defined relative to the subcell. For $TaTe_4$, the superlattice reflections appear at commensurate positions and, for convenience of notation, may be completely indixed using the three modulation wavevectors $q_1 = [\frac{1}{2}a^*, \frac{1}{2}b^*, \frac{2}{3}c^*]$, $q_2 = [\frac{1}{2}a^*, 0, \frac{2}{3}c^*]$ and $q_3 = [0, \frac{1}{2}b^*, \frac{2}{3}c^*]$. Note, however, that for a suitably transformed coordinate system Budkowski *et al* [24] have shown that a single q is also sufficient to completely describe the superstructure of $TaTe_4$.

Measurement of the satellite positions in the EDPs reveals that a commensurate to incommensurate phase transition occurs in the $Ta_{1-x}Nb_xTe_4$ system for $x \geqslant 0.3$. Below the critical Nb concentration, the EDPs of the mixed crystals are identical to those of $TaTe_4$. The commensurate to incommensurate transition is marked by an abrupt change in the c component of the q_1 wavevector (retaining for convenience the notation used for $TaTe_4$) to $q_{1c} = 0.6731 \pm 0.0012$ while the q_2 and q_3 satellites remain centred at the commensurate positions. The uncertainty in q_{1c} quoted here represents the standard deviation obtained from measurements on several different crystals of similar composition, as will be discussed below. Although only about 1%, the incommensurability may be easily observed in the EDPs. For example, in the [010] zone axis orientation (figure 2(a)), the incommensurate nature of the modulation results in a detectable zigzag of the satellite rows parallel to b^*. In the [130] zone axis *EDP* (figure 2(b)), the incommensurability is indicated by the presence of satellite doublets which arise due to the shifts of the third-order ($m = 3$) reflections from their commensurate positions. The separation of these doublets is thus directly proportional to the amount of incommensurability. As is evident in figure 2(a), the satellites associated with wavevectors q_2 and q_3 remain easily detectable for Nb concentrations near $x = \sim 0.3$. These satelites are, however, slightly broadened in comparison with the corresponding q_1-type reflections. We propose that the electron diffraction observations are the result of the development of an incommensurate phase having basal plane dimensions ($2a \times 2a$).

As x increases, further changes occur in the positions and appearance of the satellites in the EDPs. The satellites associated with q_2 and q_3 become progressively fainter and more diffuse with increasing Nb concentration while the q_1 satellites in all cases remain sharp (figures 2(c) and (d)). Note that for the end member of the series $NbTe_4$, and q_2 and q_3 satellites are replaced by very diffuse circular spots [1, 7, 9].

Following the abrupt commensurate to incommensurate transition at $x \approx 0.3$, the incommensurability of the mixed crystals has been found to vary systematically approach that observed for $NbTe_4$ as x increases. To investigate the nature of the dependence of the modulation periodicity on x, EDPs were obtained from a large number of crystals of various compositions. The exact composition of the crystals in the regions from which the EDPs were obtained was determined by EDX analysis (the estimated uncertainty for

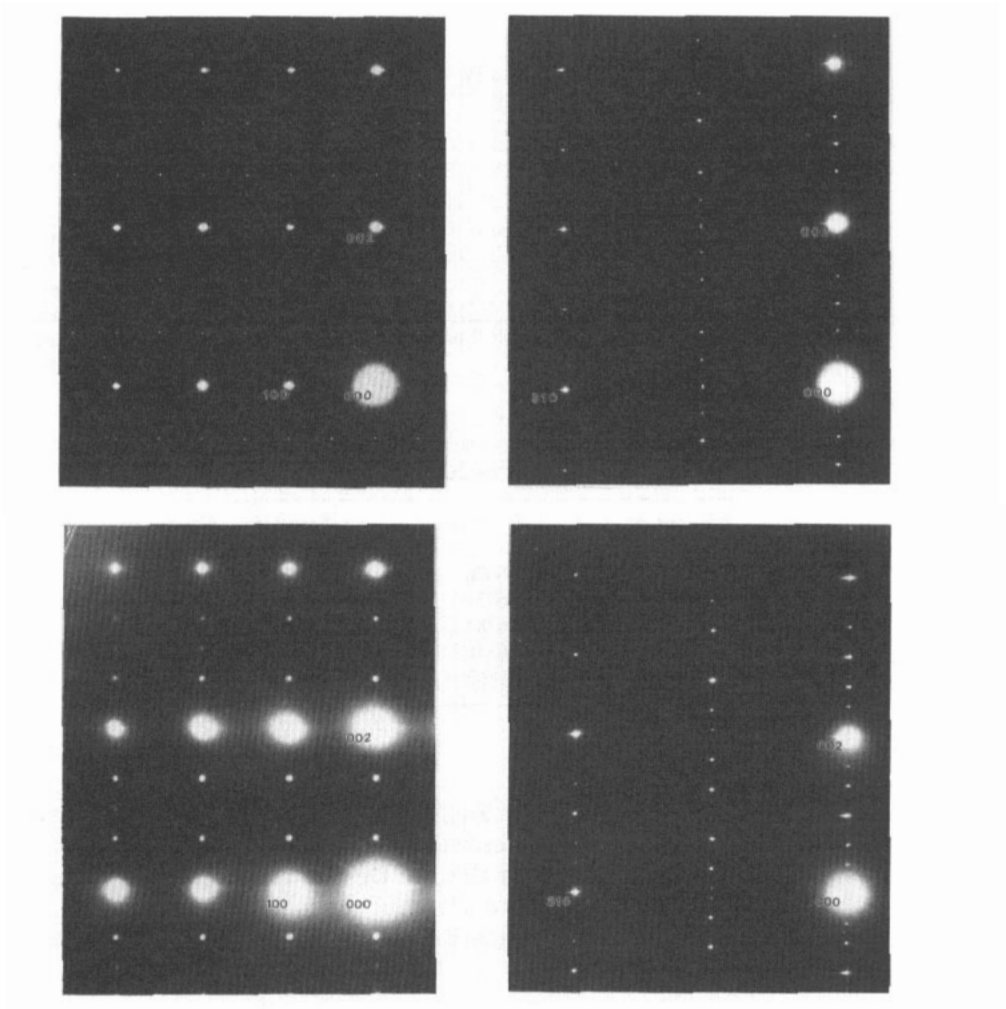

Figure 2. Selected-area electron diffraction patterns from $Ta_{1-x}Nb_xTe_4$. (*a*) [010] and (*b*) [130] zone axis patterns for $x \simeq 0.3$; (*c*) [010] and (*d*) [130] zone axis patterns for $x \simeq 0.7$.

the cations being about ±5%). Figure 3 shows the observed variation in q_{1c} with x. The variation appears to be discontinuous, proceeding through a sequence of discrete jumps as the Nb content exceeds certain threshold levels. In figure 3, the measured q_{1c} are clustered primarily around five values. Using a least-squares technique, the best estimates of the values of q_{1c} corresponding to each step were obtained. The derived values are summarized in table 1 and shown in figure 3 as a dotted line. The uncertainties in table 1 represent the standard deviation of the measured q_{1c} about the best estimate obtained from the least-squares fitting. In all cases, these uncertainties are much smaller than the size of the jumps between plateaux in q_{1c}. The plateaux are not very sharply defined. However, we note that a similar variability in the measured $\boldsymbol{q}$ has previously been reported for pure $NbTe_4$ [19] with differences of up to 1% occurring between crystallites from the same growth batch. Possible causes of the variability include the

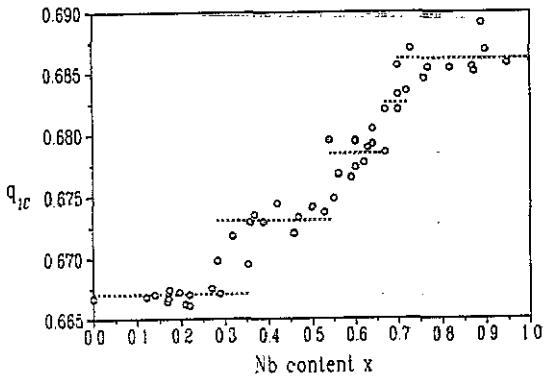

Figure 3. Variation of the modulation q with Nb content in $Ta_{1-x}Nb_xTe_4$. Open circles represent experimental measurements; ––– lines of best fit obtained from a least-squares analysis. The values of q_{1c} corresponding to the dashed lines are summarized in table 1.

Table 1. Variation of the modulation periodicity in $Ta_{1-x}Nb_xTe_4$.

Nb content	Estimated q_{1c}	Standard deviation
$0.00 \leq x \leq 0.30$	0.6670	0.0008
$0.30 \leq x \leq 0.55$	0.6731	0.0012
$0.55 \leq x \leq 0.65$	0.6784	0.0013
$0.65 \leq x \leq 0.75$	0.6826	0.0007
$0.75 \leq x \leq 1.00$	0.6862	0.0013

presence of metal-atom vacancies and/or trace impurities. Although the origin of the variability in $NbTe_4$ remains unclear, we suggest that a similar effect occurs for the mixed crystals and is intrinsic to these materials. Despite this, clustering of the measured q around particular values remains evident for the ($Ta_{1-x}Nb_xTe_4$) system. We propose that the plateaux indicate the existence of a series of long-period commensurate phases in the $Ta_{1-x}Nb_xTe_4$ system.

3.1.2. Satellite dark-field microscopy. SDF images of crystals of $TaTe_4$ rapidly cooled from the growth temperature typically reveal a three-dimensional network of APBs in the room-temperature modulation structure [5–7]. The two main types of boundaries may be distinguished in these images. Type I boundaries are generally constrained to lie parallel to the c-axis of the crystal and are out of contrast in SDF images formed using a q_1 satellite. The type II boundaries are generally inclined to the c-axis and exhibit contrast for all satellite reflections. From the observed diffraction contrast and an analysis of high-resolution images, Boswell *et al* [5] have determined the displacement vectors associated with these boundaries to be of the form $\boldsymbol{R}_1 = \frac{1}{2}\{110\}$ for type I and $\boldsymbol{R}_2 = \frac{1}{6}\{302\}$ for type II. Similar boundaries have been observed in the low-temperature commensurate phase of $NbTe_4$ [9]. In both compounds, the APBs arise due to phasing errors of the CDW on adjacent columns following a transition from a ($\sqrt{2}a \times \sqrt{2}a$) to a ($2a \times 2a$) base unit cell. SDF images of both $TaTe_4$ [6] and $NbTe_4$ [7–9] reveal that, upon heating above the C to IC phase transition temperature, the APBs gradually evolve into multiple lines similar to those previously associated with the presence of discommensuration walls in other materials [9]. Ultimately, a regular fringe-like array of discommensuration walls is observed spaced about 52 Å apart for the room-temperature

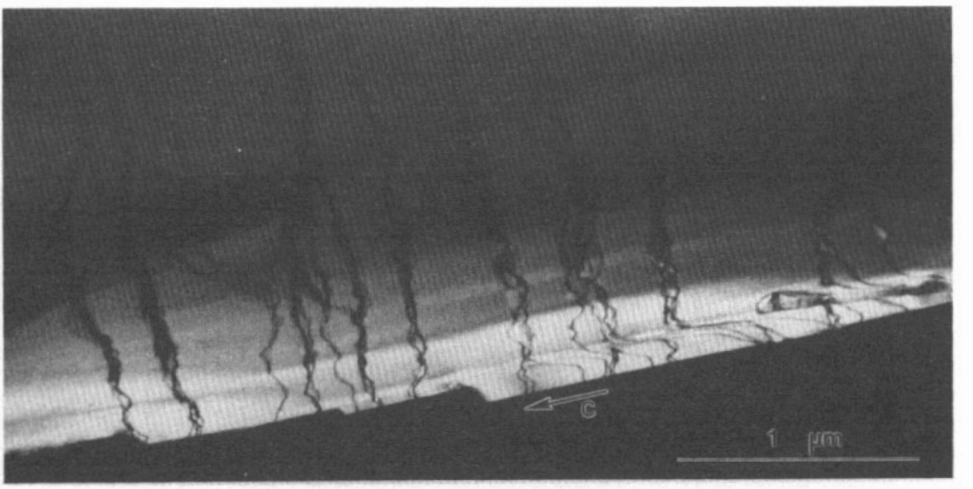

Figure 4. Satellite dark-field image formed using a q_2-type satellite of a $Ta_{1-x}Nb_xTe_4$ ($x = 0.2$) crystal showing antiphase boundaries.

incommensurate phase of $NbTe_4$ and about 200 Å apart for the high-temperature (i.e. $T > 550$ K) incommensurate phase of $TaTe_4$.

Defects are also observed in SDF images of the mixed crystals $Ta_{1-x}Nb_xTe_4$. For dopant concentrations up to about $x = 0.3$, the modulation periodicity is unchanged, remaining commensurate, while the SDF images (figure 4) reveal the presence of APBs similar to those observed in quenched $TaTe_4$. However, since the mixed crystals were slow-cooled, these APBs are probably associated with pinning of the CDW phases along the various columns by the impurities (i.e. the Nb atoms). The number of APBs has been found to increase roughly in proportion to the level of substitution, in agreement with this proposal. Effects attributed to local pinning of the phase of a CDW by impurities have also been noted in several of the transition metal di- and trichalcogenides [25, 26]. The fact that a large concentration of Nb ions may be introduced into $TaTe_4$ without altering the modulation periodicity indicates that the interaction between the CDW phase and the impurity potential is quite weak, as expected for a nominally isoelectronic substitution of this type.

Increasing the Nb concentration beyond $x \simeq 0.3$ results in a commensurate to incommensurate phase transition and is accompanied by characteristic changes in the nature of the defects observed in the SDF images. As described above, for Nb concentrations slightly in excess of the threshold, the satellites associated with q_2 (or equivalently q_3) are sufficiently intense to allow the formation of a SDF image. These images reveal APBs apparently similar to those occurring in the commensurate Nb-doped crystals and quenched $TaTe_4$ except that the boundaries are present with a much greater density (figure 5(*a*)). In SDF images of the same crystal formed using a q_1-type satellite (figure 5(*b*)), however, the APBs exhibit very weak or vanishing contrast. In place of the APBs, a patchwork of irregularly shaped domains is typically observed. The explanation of this diffraction contrast remains unclear. We note that the appearance of the domains is very sensitive to the specimen tilt (i.e. the deviation parameter) suggesting that lattice strains, possibly associated with the APBs, influence the observed diffraction contrast. Contrast effects attributed to the strain associated with type I APBs in room-temperature $TaTe_4$

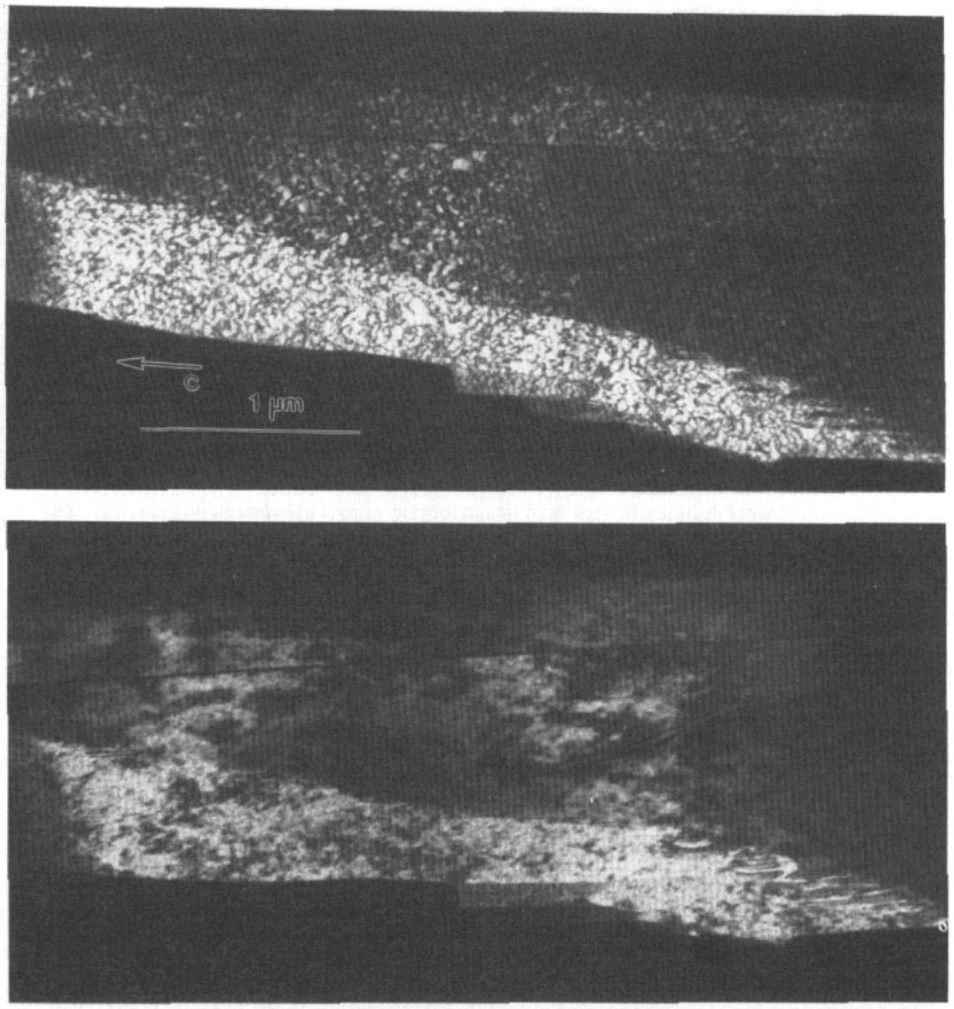

Figure 5. Satellite dark-field images of the same region of a $Ta_{1-x}Nb_xTe_4$ ($x \simeq 0.3$) crystal formed using (*a*) a $\boldsymbol{q}_2$-type satellite and (*b*) a $\boldsymbol{q}_1$-type satellite.

have previously been reported [5]. A high density of overlapping APBs and their accompanying strains under dynamical diffracting conditions might account for the complicated diffraction contrast observed, but detailed calculations are needed to confirm this. The lack of any domain contrast of this type for $TaTe_4$ and $NbTe_4$ again implies that the defects arise from pinning of the CDW phases by impurities. Alternatively, the observed APB contrast may simply indicate that the associated displacement vectors differ from those found in the commensurate structures. Boswell *et al* [5] have previously shown that, for the room-temperature phase of $Tate_4$, displacive boundaries of the form $\boldsymbol{R} = \frac{1}{2}[100]$ (type III), although not observed experimentally, are possible from a geometrical standpoint. Since the mixed crystals retain the $(2a \times 2a)$ basal dimensions of room-temperature $TaTe_4$, type III APBs would also seem to be a possibility for these compounds. A network of APBs consisting of types I and III would be consistent with the observed diffraction contrast.

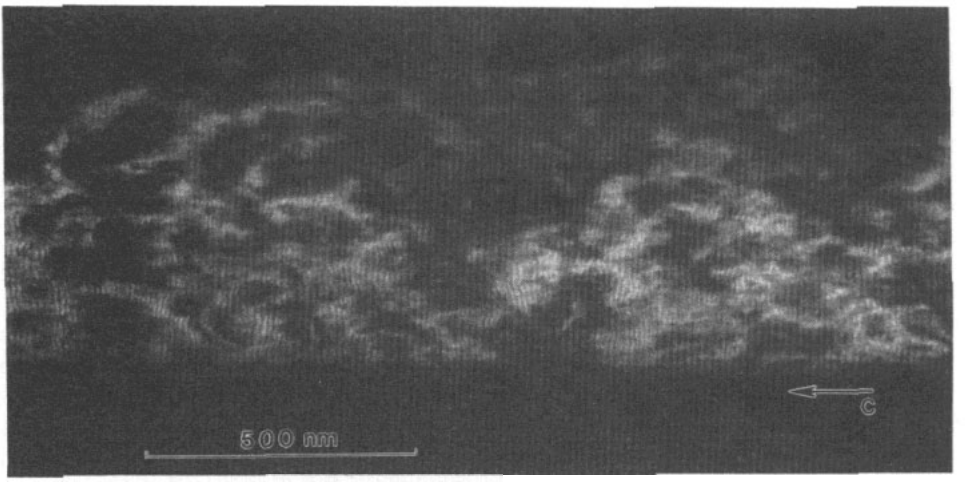

Figure 6. Satellite dark-field image of a $Ta_{1-x}Nb_xTe_4$ ($x \simeq 0.6$) crystal formed using a q_1-type satellite, showing regularly spaced fringes about 100 Å apart.

In the incommensurate phases of the mixed crystals, the SDF images obtained using a q_1-type satellite also generally show an array of closely spaced fringes perpendicular to the *c*-axis superposed on the irregular domain pattern (figure 6). Similar fringes have previously been observed in SDF images of the room-temperature phase of $NbTe_4$ [7–9] and have been interpreted as arising from the presence of an array of discommensuration walls (i.e. the projection of all the one-dimensional discommensurations in a plane normal to the *c*-axis). The average spacing of the fringes was observed to vary from about 250 Å for compositions corresponding to the first plateau in figure 3 to about 50 Å for Nb contents near $x = 1.0$. Unlike the uniform fringes observed for $NbTe_4$, in all of the mixed crystal phases the fringes are 'wavy', exhibiting significant variations in orientation and, to a lesser degree, in spacing. Some of this disorder may be related to the presence of pinning points arising from small variations in stoichiometry. However, although the APBs do not show any contrast in SDF images formed with this type of satellite, the fringes are also often displaced on crossing over the location of the (out of contrast) boundaries accounting for a large part of the orientational variation. The fringe-like arrays become progressively more regular as x increases. Since the q_2 and q_3 satellites also broaden into diffuse regions as x increases, this scattering effect is apparently unrelated to any disorder in the discommensuration arrays.

3.2. Observations above room temperature

EDPs obtained at elevated temperatures indicate the occurrence of CDW-driven structural transitions in several of the mixed crystal phases. For crystals containing relatively small amounts of Nb, up to $x \simeq 0.2$, a transition from the $(2a \times 2a \times 3c)$ room-temperature commensurate phase to a $(\sqrt{2}a \times \sqrt{2}a \times 3c)$ commensurate phase occurs near 450 K. This behaviour is identical to that previously reported for $TaTe_4$.

For the commensurate crystals containing near, but slightly less than, the critical Nb concentration of $x \simeq 0.3$, two distinct phase transitions are observed. A C to IC transition occurs upon heating at about 350 K in which the value of q_{1c} changes discontinuously to 0.672 ± 0.001. This value of q_{1c} exactly corresponds to that of the second plateau in the

observed room-temperature dependence of q_1 on the Nb content (i.e. for $0.3 \leqslant x \leqslant 0.55$ in figure 3). Apparently, at elevated temperatures smaller amounts of Nb are needed to stabilize the incommensurate phase. The observation of this phase transition provides further indirect evidence for the proposed stepwise variation of q with x at room temperature. SDF images obtained during the commensurate to incommensurate phase transition are shown in figure 7. In the commensurate state, relatively few APBs, mainly of type II, are observed in SDF images formed using a q_2-type satellite (figure 7(*a*)). On heating into the incommensurate state, a network of APBs forms in all regions of the crystal (figure 7(*b*)). This process is generally completed within a few seconds. For SDF images formed using a q_1-type satellite, the diffraction contrast of the defects changes from APB contrast in the commensurate state to a superposed patch-like domain and fringe contrast in the incommensurate state (figure 7(*c*)), similar to that decribed previously. Considerable temperature hysteresis occurs between warming and cooling for this transition. On cooling in the microscope from 350 K, the incommensurate state persists to room temperature with no observable changes occurring in either the EDPs or SDF images. However, a very sluggish transition back to the commensurate state does occur at room temperature over a period of several hours. SDF images indicate that the number of APBs is greatly reduced, to near the original density, during this transition (figure 7(*d*)). Upon further heating to about 450 K, a sharp reversible incommensurate to incommensurate transition takes place. The disappearance of the q_2 and q_3 satellites in the EDPs indicates a structural transformation to a new phase with basal plane dimensions ($\sqrt{2}a \times \sqrt{2}a$). SDF images formed using these satellites show the phase transition is initiated at the APBs which progressively broaden and ultimately expand to convert the entire crystal to dark contrast (i.e. to the $\sqrt{2}a$ phase). Very similar phenomena have been reported for $TaTe_4$ [5, 6] during the commensurate to commensurate phase transition in that compound. On further heating, no change in the incommensurability (i.e. the magnitude of q_{1c}) was observed until the crystals began to distintegrate (at about 650 K under the conditions prevailing in the electron microscope).

For the mixed crystal compositions which are already incommensurate at room temperature (i.e. those with $x \geqslant \sim 0.3$), an incommensurate to incommensurate transition similar to that described above has also been observed at about 450 K. SDF images show that the fringes associated with the discommensuration arrays are more regular above 450 K and again suggests that interactions with the APBs contribute to the orientational variation observed at lower temperatures. The incommensurability has also been found to be temperature-independent in these crystals.

Attempts were made to observe a lock-in transition for the incommensurate phases by cooling below room temperature. No changes occurred in the satellite positions down to the lowest temperature obtainable (about 30 K), although the diffuse satellites became more streaked on cooling. No finely spaced satellites were observed along the streaks analogous to those of the LT_1/LT_2 phases of $NbTe_4$.

4. Discussion

4.1. A model for the long-period modulated structures of $Ta_{1-x}Nb_xTe_4$

The electron diffraction study of $Ta_{1-x}Nb_xTe_4$ gives a clear indication of a stepwise variation of the CDW modulation wavevector q as a function of composition. Thus it appears justified to consider the superstructure corresponding to each step as long-period

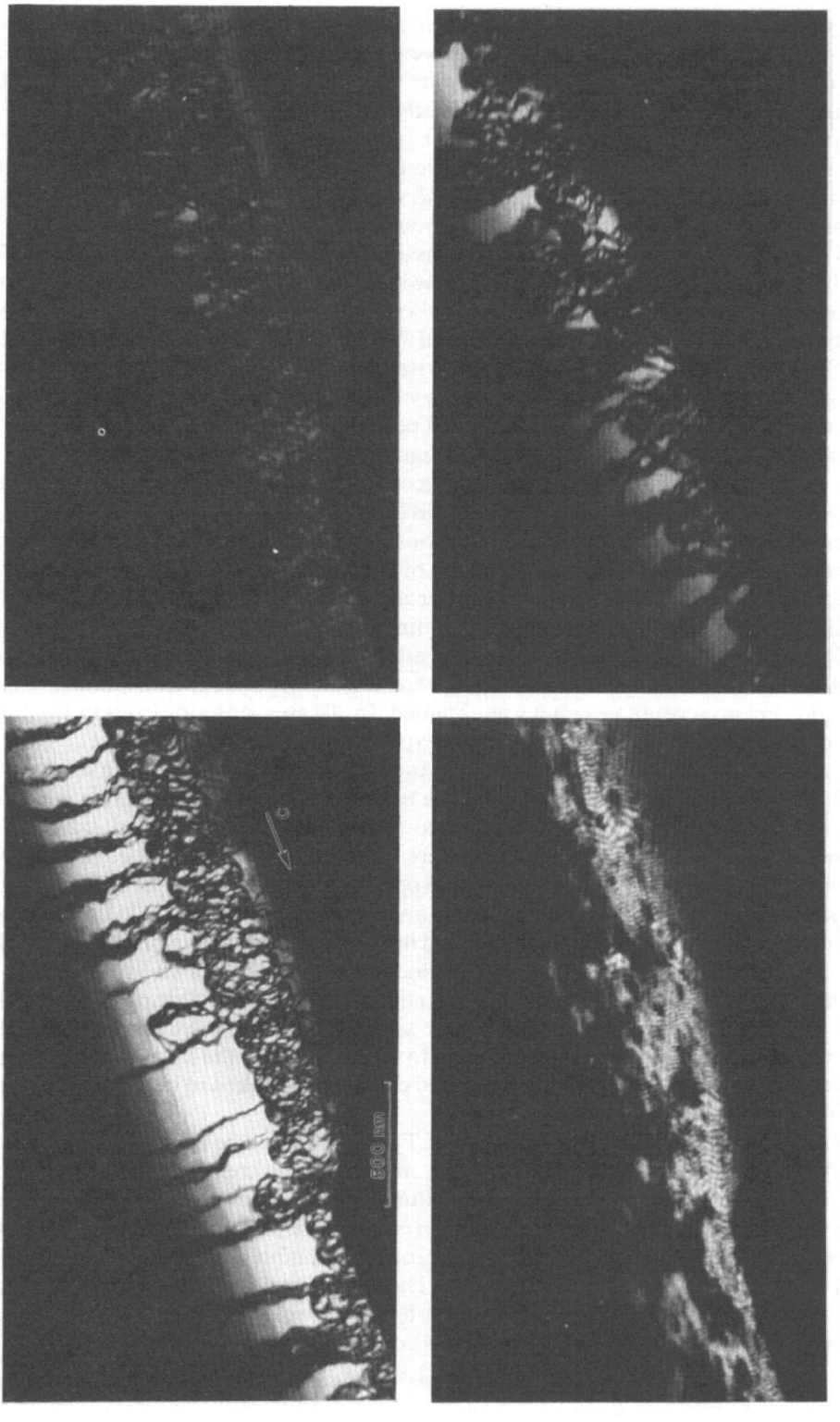

Figure 7. Satellite dark-field images of the same region of a $Ta_{1-x}Nb_xTe_4$ ($x \approx 0.2$) crystal formed using a q_2-type satellite. Top left: at room temperature, top right at about 350 K, bottom left: cooled to room temperature (after a period of several hours) and bottom right: formed using a q_1-type satellite at about 350 K.

commensurate (LPC) rather than incommensurate. The solution of these structures by conventional x-ray methods is difficult, however, since the satellite reflections are often broadened and have relatively low intensities. To obtain a best approximation regarding the nature of the modulation, models of the superstructures have been studied by comparison of the observed and computer simulated EDPs. This approach is a direct extension of our previous description of the LT_1/LT_2 phases of $NbTe_4$ [11] where the separation of the weak, heavily streaked and very closely spaced satellites was similarly beyond the capability of conventional x-ray analysis.

The calculation† of the satellite positions and intensities in the EDPs of $Ta_{1-x}Nb_xTe_4$ was based upon that recently used for the two low-temperature $NbTe_4$ phases which, it is now apparent, constitute the end members of the series. Based on the observed periodicities, the unit cell of the hypothetical average structure was enlarged to $A = B = 2a$, $C = 384c$ for the calculations and comprised four MTe_4 columns. This choice for the unique axis length is the smallest multiple of that used for the LT_1/LT_2 calculation, $32c$, which accommodates all the observed periodicities in the $Ta_{1-x}Nb_xTe_4$ system as discussed further below. The original average structure positions ($2a$ for M and $8m$ for Te in space group $P4/mcc$) were changed according to the modulation function given by van Smaalen [4] for room-temperature $NbTe_4$. First- and second-order modulation harmonics are considered in the calculations. No attempt was made to differentiate between Nb or Ta atoms in the calculation of the EDPs, but, assuming that no ordering occurs, the differences in scattering power of the metal atoms should generate only relatively small discrepancies in the magnitudes of the intensities calculated for the satellites and therefore do not significantly affect the results of the analysis. In order to confirm this, a number of calculations were also carried out incorporating Ta–Nb ordering, but no acceptable result was obtained. In all cases, ordering leads to additional superstructure reflections which were not experimentally observed.

The main modulation is a 'breathing' mode distortion along all of the columns. In order to enlarge the unit cell from the $\sqrt{2}a$ base of $NbTe_4$ to a $2a$ base, two additional deformation modes, previously referred to as LT_1 and LT_2 by Prodan *et al* [5], are required. Other possible deformations were considered but did not yield satisfactory agreement between the calculated and experimentally observed EDPs. For the LT_1 distortion, half of the columns (columns III and IV after the notation of [5]), which were originally in phase, are alternatively shifted in opposite directions along the c axis. The LT_2 distortion involves further alternate clockwise and anticlockwise rotations of the Te cages around the c-axis superimposed on the breathing mode distortion. As a result, the LT_2 modulation results in an effective extension of the Te cages. The four LT_2 columns are interrelated by a 4_1 screw axis. In the calculation, the amplitudes of the LT_1 and LT_2 shifts (δ_1 and δ_2 in [5]) for the mixed crystals were taken to be the same as those occurring in $NbTe_4$.

Briefly, the physical significance of the LT_1 distortion can be understood in terms of the following. In room-temperature $NbTe_4$, the Nb atoms are predominantly grouped into triplets along the columns but other multiplets (e.g. doublet–singlet sequences) are also present. The effect of the LT_1 distortion is to emphasize triplet formation along the chains. In room-temperature $TaTe_4$, this process is complete with each column being comprised entirely of Ta atom triplets. The LT_1 distortion generates atomic displacements similar to those found in room-temperature $TaTe_4$ and thus may be considered a precursor to the formation of this commensurate phase. In pure $NbTe_4$, low

† The source program listing and decription has been deposited with the British Library as Supplementary Publication SUP 52947.

temperatures are required to stabilize the LT_1/LT_2 phases. Our calculations indicate that the superstructures of the $Ta_{1-x}Nb_xTe_4$ series may be interpreted in terms of the presence of LT_1-type and LT_2-type distortions at room temperature.

The electron diffraction observations indicate the occurrence of a stepwise variation in the CDW periodicity as a function of composition in $Ta_{1-x}Nb_xTe_4$. Calculations were

Table 2. Calculated intensities (I) for $Ta_{1-x}Nb_xTe_4$. Intensities are rounded up the first digit. $\delta_1 = 6.67E-7$ for the LT_1 type of distortion and $\delta_2 = 3.E-2$ for the LT_2 type of distortion. All calculations were carried out for a ($2a \times 2a$ 384c) unit cell.

$TaTe_4$			$Nb_{1/4}Ta_{3/4}Te_4$			$Nb_{1/2}Ta_{1/2}Te_4$			$Nb_{3/4}Ta_{1/4}Te_4$			$NbTe_4LT_1/LT_2$		
h k l		I	*h k l*		I	*h k i*		I	*h k l*		I	*h k l*		I
0 0 0		2.E+8	0 0 0		2.E+8	0 0 0		2.E+8	0 0 0		2.E+8	0 0 0		2.E+8
0 0 256		2.E+4	0 0 252		6.E+1	0 0 248		6.E+1	0 0 244		5.E+	0 0 240		2.E+4
												0 0 288		2.E+0
												0 0 480		7.E+1
0 0 512		1.E+3	0 0 516		2.E+3	0 0 520		2.E+3	0 0 524		2.E+3	0 0 528		9.E+2
												0 0 720		6.E−1
0 0 768		8.E+7	0 0 768		7.E+7	0 0 768		7.E+7	0 0 768		7.E+7	0 0 768		8.E+7
												1 0 12	δ_2	3.E−1
												1 0 240	δ_1	1.E+0
1 0 256	$\delta_1+\delta_2$	2.E+4	1 0 255	δ_2	1.E−1	1 0 254	δ_2	1.E−1	1 0 253	δ_2	1.E−1	1 0 252	δ_2	1.E−1
			1 0 258	δ_1	1.E+0	1 0 260	δ_1	1.E+0	1 0 262	δ_1	1.E+0	1 0 264	δ_1	1.E+0
												1 0 276	δ_2	1.E−1
			1 0 510	δ_1	3.E−1	1 0 508	δ_1	4.E−1	1 0 506	δ_1	4.E−1	1 0 504	δ_1	2.E−1
1 0 512	$\delta_1+\delta_2$	1.E+3	1 0 513	δ_2	1.E−1	1 0 514	δ_2	1.E−1	1 0 515	δ_2	1.E−1	1 0 516	δ_2	1.E−1
			1 0 516	δ_1	1.E−1	1 0 520	δ_1	1.E−1	1 0 524	δ_1	1.E−1			
												1 0 744	δ_1	1.E+0
												1 0 756	δ_2	3.E−1
			3 0 3	δ_2	3.E+1	3 0 6	δ_2	3.E+1	3 0 9	δ_2	3.E+1	3 0 12	δ_2	3.E+1
3 0 256	$\delta_1+\delta_2$	3.E+4	3 0 255	δ_2	3.E+1	3 0 254	δ_2	3.E+1	3 0 253	δ_2	3.E+1	3 0 252	δ_2	3.E+1
			3 0 258	δ_1	2.E+0	3 0 260	δ_1	2.E+0	3 0 262	δ_1	2.E+0	3 0 264	δ_1	2.E+0
			3 0 262	γ_2	1.E−1									
3 0 512	$\delta_1+\delta_2$	2.E+3	3 0 510	δ_1	1.E+0	3 0 508	δ_1	1.E+0	3 0 506	δ_1	1.E+0	3 0 504	δ_1	1.E+0
			3 0 513	δ_2	3.E+1	3 0 514	δ_2	3.E+1	3 0 515	δ_2	3.E+1	3 0 516	δ_2	3.E+1
3 0 768	$\delta_1+\delta_2$	8.E−1	3 0 765	δ_2	3.E+1	3 0 762	δ_2	3.E+1	3 0 759	δ_2	3.E+1	3 0 756	δ_2	3.E+1
												2 1 12	δ_2	3.E−1
			2 1 126	δ_1	8.E−1	2 1 124	δ_1	8.e−1	2 1 122	δ_1	1.E+0	2 1 120	δ_1	8.E−1
2 1 128	$\delta_1+\delta_2$	3.E+3	2 1 129	δ_2	1.E−1	2 1 130	δ_2	1.E−1	2 1 131	δ_2	1.E−1			
												2 1 144	δ_2	1.E−1
												2 1 240	δ_1	1.E−1
2 1 256	$\delta_1+\delta_2$	3.E+2										2 1 276	δ_2	7-E−1
												2 1 492	δ_2	7.E−1
2 1 512	$\delta_1+\delta_2$	9.E+3	2 1 510	δ_1	7.E−1	2 1 508	δ_1	7.E−1	2 1 506	δ_1	7.E−1	2 1 504	δ_1	4.E−1
			2 1 516	δ_1	1.E−1	2 1 520	δ_1	1.E−1	2 1 524	δ_1	1.E−1	2 1 528	δ_1	4.E−1
												2 1 624	δ_1	1.E−1
2 1 640	$\delta_1+\delta_2$	2.E−1	2 1 639	δ_2	1.E−1	2 1 638	δ_2	1.E−1	2 1 637	δ_2	1.E−1			
			2 1 642	δ_1	2.E+0	2 1 644	δ_1	2.E+0	2 1 646	δ_1	2.E+0	2 1 648	δ_1	3.E+0
												2 1 756	δ_2	4.E−1
1 1 256		2.E+4	1 1 258		1.E+4	1 1 260		1.E+4	1 1 262		1.E+4	1 1 264		2.E+4
1 1 512		6.E+3	1 1 510		1.E+4	1 1 508		1.E+4	1 1 506		1.E+4	1 1 504		8.E+4
												1 1 552		1.E+0
1 1 768			1 1 762		4.E+1	1 1 756		4.E+1	1 1 750		4.E+1	1 1 744		4.E+3
2 4 0		2.E+6	2 4 0		2.E+6	2 4 0		2.E+6	2 4 0		2.E+6	2 4 0		2.E+6
2 4 128		7.E+2	2 4 132		2.E+3	2 4 136		2.E+3	2 4 140		2.E+3	2 4 144		2.E+3
2 4 256		8.E+4	2 4 252		2.E+2	2 4 248		2.E+2	2 4 244		2.E+2	2 4 240		1.E+2
2 4 384		7.E+7	2 4 384		7.E+7	2 4 384		7.E+7	2 4 384		7.E+7	2 4 384		7.E+7
2 4 512		1.E+5	2 4 516		3.E+3	2 4 520		3.E+3	2 4 524		3.E+3	2 4 528		4.E+3
2 4 640		2.E+4	2 4 636		2.E+3	2 4 632		2.E+3	2 4 628		2.E+3	2 4 624		2.E+3
2 4 768		1.E+7	2 4 768		1.E+7	2 4 768		1.E+7	2 4 768		1.E+7	2 4 768		1.E+7

carried out for a series of five LPC structures corresponding to the most apparent plateaus in the wavevector q. The number of LT_1 modulations within $384c$ was taken as 256 ($q_{1c} = 0.6667$) for $x \leqslant 0.3$, 258 ($q_{1c} = 0.6719$) for $0.3 \leqslant x \leqslant 0.55$, 260 ($q_{1c} = 0.6771$) for $0.55 \leqslant x \leqslant 0.65$, 262 ($q_{1c} = 0.6823$) for $0.65 \leqslant x \leqslant 0.75$ and 264 ($q_{1c} = 0.6875$) for $x \geqslant 0.75$ while the corresponding LT_2 values were half as large [5]. The results of the calculations are summarized in table 2. Only reflections whose calculated intensity exceeds a threshold value, determined mainly by rounding errors, are listed. The calculated satellite positions and their intensities are in good agreement with the observed EDPs for each range of compositions. Those rows of reflections were the LT_1 and LT_2 satellites do not overlap (e.g. $\langle 10l \rangle$) require a further comment. In the calculated EDPs, a few weak satellites appear in closely spaced groups with intensities determined by a sharp envelope function. The envelopes are always centred at $\frac{1}{2}c^*$ although the satellites themselves are not. The experimentally obtained EDPs show only diffuse reflections centred at $\frac{1}{2}c^*$ along these rows. This discrepancy may be accounted for, since the spacing of the predicted satellites is several times smaller than the already narrowly spaced reflections observed for the LT_1/LT_2 phases of pure $NbTe_4$ and, as such, probably not resolvable in our experiments. We note that, analogously with $NbTe_4$, the diffuse reflections become streaked on cooling, although LT_1 and LT_2 satellites along the streaks are not observed.

The symmetries of the $Ta_{1-x}Nb_xTe_4$ phases are described by the same space groups as determined for $NbTe_4$ [5]. For the main breathing mode modulation structure and its LT_1, LT_2 and combined LT_1/LT_2 distortions, the appropriate space groups are $P4/m$, $P4/n$, $I4/m$ and $P4_2/m$ respectively.

The LPC picture of the superstructures of $Ta_{1-x}Nb_xTe_4$ provides further insight into the surprisingly complex phase relationships occurring in this 'simple' system. In general, the various phases in $Ta_{1-x}Nb_xTe_4$ are stabilized by several competing factors. If possible, the metal chains are distorted by the CDW to form triplets with the largest permissible phase shift occurring between neighbouring columns. In addition, the inter- and intracolumn Te–Te bonding distances are preferentially maintained nearly constant [2, 5, 21]. For the room-temperature phase of $NbTe_4$, Nb triplets only cannot be formed and the largest possible phase difference is found between the columns, i.e. π. In the case of room-temperature $TaTe_4$, the CDW along neighbouring columns are shifted in phase by $2\pi/3$, resulting in the formation of Ta triplets exclusively. The LT-like states of $Ta_{1-x}Nb_xTe_4$ are somewhat intermediate between these two extremes. As for $NbTe_4$, nearest-neighbour columns are related in phase by π, but with a small phase shift associated with the LT_1 distortion. This effectively results in a relative phasing of $(\pi - \varphi)$ for one set of nearest-neighbour columns and $(\pi + \varphi)$ for the others, where φ is an arbitrary phase shift determined by the number of LT_1 periods fitting the enlarged unit cell. The displacements associated with the LT_1 distortion result in progressively more of the metal atoms being grouped into triplets. Since the number of LT_1/LT_2 periods in the extended unit cell must be an integer, the possible phase shifts φ between the columns are restricted to certain discrete values. This is also probably related to the phasing relationships imposed by intercolumnar bonding.

The properties of incommensurate systems have generated intense theoretical interest. In particular, the response of the modulation wavevector q to changes in some parameter such as temperature or composition has been studied in detail [22, 27, 28]. The theoretical analyses indicate that; for an 'incommensurate' system, the adoption of some proximal long period is often energetically favourable. Under certain conditions, the occurrence of a 'Devil's staircase', where q locks in to an infinity of commensurate

values, has been predicted. The observation of a series of LPC phases in $Ta_{1-x}Nb_xTe_4$ provides the first direct experimental evidence for this type of behaviour in a CDW modulated system (Borodin *et al* [29] have also interpreted phenomena observed in the electrical properties of orthorhombic TaS_3 in terms of the existance of a series of metastable incommensurate phases). In $Ta_{1-x}Nb_xTe_4$, since q assumes only a finite number of commensurate values, this system represents an example of a 'harmless staircase' [30].

Based on expansions of the Landau free energy, Walker and co-workers [13–17] have developed a theoretical framework to describe the phase transitions in $NbTe_4$ and $TaTe_4$. In all cases, the driving mechanism for the transitions involves variations in the relative strengths of first-, second- and third-neighbour intercolumn interactions. Only variations of the interaction strengths with temperature were considered in this analysis, however. It appears that changes in the stoichiometry of the crystals produce similar variations in the intercolumn interaction strengths. Variations may arise from local distortions of the intercolumn Te–Te bonding associated with the substitution of Nb for Ta ions.

4.2. *Discommensurations and* APBs

SDF imaging reveals that discommensurations and APBs play an important role in the 'incommensurate' (LPC) phases of $Ta_{1-x}Nb_xTe_4$. As shown by Mahy *et al* [9] for $NbTe_4$, the discommensurations involve displacements of the form $\boldsymbol{R} = \frac{1}{8}\langle 302\rangle$. For the commensurate phases ($x \leqslant 0.3$), APBs involving similar displacements have also been observed. These two types of defects are clearly closely related, differing primarily in the abruptness of the associated phase slip. For an APB, the phase slip is by definition restricted to the immediate vicinity of the interface. However, the nature of the phase slip associated with discommensurations in this system is unclear. In the LPC models of the structures, second-order harmonics are included in the modulation function generating the atomic displacements and, as a consequence, discommensurations appear along the columns as multiplets of a different nature than the predominant triplet sequence. The discommensuration comprises a sequence of approximate doublet-single groupings and thus the phase slip occurs gradually over a considerable spatial extent. This picture of the discommensurate state is in agreement with the high-resolution imaging studies of the room-temperature phase of $NbTe_4$ which found very little evidence of phase slip associated with the discommensurations [7, 9].

APBs are observed in both the commensurate and incommensurate (LPC) phases of $Ta_{1-x}Nb_xTe_4$. In the commensurately modulated compounds, the APBs represent stacking faults between otherwise identical commensurate domains, while those in the incommensurate phases presumably separate identical incommensurate domains. Interaction with these APBs is at least partially responsible for the observed orientational and spatial variations of the discommensuration arrays. The APBs also play a significant role in the commensurate to incommensurate transition which occurs on heating $Ta_{1-x}Nb_xTe_4$ ($0.2 \leqslant x \leqslant 0.3$) above about 350 K. This transition is accompanied by a rapid increase in the number of boundaries. According to the LPC interpretation of the structures, the relative phasing of the CDW on nearest-neighbour columns changes from $2\pi/3$ to about π as a result of this transition. The observed generation of a large number of APBs implies that the atomic displacements necessary to achieve this reshuffling of phases cannot be easily accomplished, possibly due to impurity pinning (in this case Nb ions) of the CDW. The commensurate to incommensurate transition occurs very rapidly.

However, the reverse incommensurate to commensurate process is sluggish, requiring several hours for completion at room temperature. A similarly sluggish lock-in transition has been observed for $NbTe_4$ and is apparently characteristic for this system. This indicates that formation of the metal-atom triplet sequences during lock-in, and the attendant removal of the discommensuration arrays, is a very slow process independent of the temperatures at which it occurs. It is interesting to note that the subsequent incommensurate to incommensurate transition occurring at around 450 K, as well as the previously reported commensurate to commensurate transition in $TaTe_4$, both of which involve substantial rearrangements of the CDW phasings along the columns as the unit cell changes from $(2a \times 2a)$ to $(\sqrt{2}a \times \sqrt{2}a)$ base but which in neither case require the formation or break-up of triplet groupings, occur rapidly without any significant temperature hysteresis.

5. Conclusion

The study of the $Ta_{1-x}Nb_xTe_4$ system provides many new insights regarding the character of CDW states in general and the transitions between them. The interrelationship of what initially appear quite different phenomena in the extensively studied transition metal tetrachalcogenides $TaTe_4$ and $NbTe_4$ can now be understood within the context of a series of LPC phases. The stepwise nature of the transition between the LPC phases in $Ta_{1-x}Nb_xTe_4$ provides the first direct experimental evidence in a CDW modulated material for the Devil's staircase that is predicted to occur under certain conditions in incommensurate systems. In addition, the numerous unusual aspects of the CDW behaviour in these materials, including the sluggishness of the lock-in transitions, the role of APBs in the transitions and the anomalous diffraction contrast of these APBs, challenge our understanding of the CDW state and await further investigation.

Acknowledgments

This work was financially supported by the Ministry for Research and Technology of the Republic of Slovenia (AP) and the Natural Sciences and Engineering Research Council of Canada. Technical assistance by Z Skraba and P Stillwell is gratefully acknowledged.

References

[1] Boswell F W, Prodan A and Brandon J K 1983 *J. Phys. C: Solid State Phys.* **16** 1067
[2] Bronsema K D, van Smaalen S, de Boer J, Wiegers G A and Jellinek F 1987 *Acta Crystallogr.* B **43** 305
[3] Böhm H and Von Schnering H G 1985 *Z. Kristallogr.* **171** 41
[4] van Smaalen S, Bronsema K D and Mahy J 1986 *Acta Crystallogr.* B **42** 43
[5] Boswell F W, Prodan A, Bennett J C, Corbett J M and Hiltz L G 1987 *Phys. Status Solidi* A **102** 207
[6] Bennett J C, Boswell F W, Prodan A, Corbett J M and Ritchie S 1991 *J. Phys. C: Solid State Phys.* **3** 6959
[7] Eaglesham D J, Bird D, Withers R L and Steeds J W 1985 *J. Phys. C: Solid State Phys.* **18** 1
[8] Mahy J, van Landuyt J, Amelinckx S, Uchida Y, Bronsema K D and van Smaalen S 1985 *Phys. Rev. Lett.* **55** 11
[9] Mahy J, van Landuyt J, Amelinckx S, Bronsema K D and van Smaalen S 1986 *J. Phys. C: Solid State Phys.* **19** 5049
[10] Boswell F W and Prodan A 1986 *Phys. Rev.* B **34** 2979

[11] Prodan A, Boswell F W, Bennett J C, Corbett J M, Vidmar T, Marinkovic V and Budkowski A 1990 *Acta Crystallogr.* B **46** 587
[12] MacMillan W L 1975 *Phys. Rev.* B **12** 1187
[13] Walker M B 1985 *Can. J. Phys.* **63** 46
[14] Sahu D and Walker M B 1985 *Phys. Rev.* B **32** 1643
[15] Walker M B and Morelli R 1988 *Phys. Rev.* B **38** 4826
[16] Morelli R and Walker M B 1989 *Phys. Rev. Lett.* **62** 1520
[17] Chen Z Y and Walker M B 1989 *Phys. Rev.* B **40** 8983
[18] Withers R L and Wilson J A 1986 *J. Phys. C: Solid State Phys.* **19** 4809
[19] Boswell F W and Prodan A 1984 *Mater. Res. Bull.* **19** 93
[20] Bennett J C, Boswell F W, Corbett J M, Prodan A and Kohara S 1990 *Proc. 12th Int. Congress for Electron Microscopy (Seattle, WA, 1990)* (San Francisco, CA: San Francisco Press) p 170
[21] Kucharczyk D, Budkowski A, Boswell F W, Prodan A and Marinkovic V 1990 *Acta Crystalogr.* B **46** 153
[22] Bak P 1982 *Rep. Prog. Phys.* **45** 587
[23] Van Cappellan E 1986 *Proc. 11th Int. Congress on X-ray Optics and Microanalysis (London, Ontario, 1990)* ed J D Brown and R H Packwood p 409
[24] Budkowski A, Producan A, Marinkovic V, Kucharczyk D, Uszynski I and Boswell F W 1989 *Acta Crystallogr.* B **45** 529
[25] Wilson J A, DiSalvo F J and Mahajan S 1975 *Adv. Phys.* **24** 117
[26] Chaiken P M, Fuller W W, Lacoe R, Kwak J F, Greene R L, Eckert J C and Ong N P 1981 *Solid State Commun.* **39** 553
[27] Aubry S, Axel F and Vallet F 1985 *J. Phys. C: Solid State Phys.* **18** 753
[28] Evangelou S N and Economou E N 1991 *J. Phys.: Condens. Matter* **3** 5499
[29] Borodin D V, Nad F Ya, Savitskaya Ya S and Zaitsev-Zotov S V 1986 *Physica* B **143** 73
[30] Villain J and Gordon M 1980 *J. Phys. C: Solid State Phys.* **13** 3117